J. Math. Anal. Appl. 460 (2018) 17–32

Contents lists available at ScienceDirect

Journal of Mathematical Analysis and Applications

www.elsevier.com/locate/jmaa

Positive solutions for the Kirchhoff-type problem involving general critical growth – Part II: 3D numerical solutions

Cong Gu [a,*], Chun-Ming Yang [b], Tai-Chia Lin [b], Jean Yeh [a], Huixing Zhang [c]

[a] Department of Mathematics, Texas A&M University, College Station, TX, USA
[b] Department of Mathematics, National Taiwan University, Taipei, Taiwan, ROC
[c] School of Mathematics, China University of Mining and Technology, Xuzhou, Jiangsu, China

ARTICLE INFO

Article history:
Received 31 May 2017
Available online 8 September 2017
Submitted by G. Chen

Keywords:
Kirchhoff-type problem
Positive solutions
Critical nonlinearity
Numerical solutions

ABSTRACT

In this paper, we continue the study of the following Kirchhoff-type problem

$$\begin{cases} \left(a+\lambda\int\limits_{\mathbb{R}^3}|\nabla u|^2dx+\lambda b\int\limits_{\mathbb{R}^3}|u|^2dx\right)(-\Delta u+bu)=f(u), \text{ in } \mathbb{R}^3, \\ u\in H^1(\mathbb{R}^3),\ u>0, \text{ in } \mathbb{R}^3, \end{cases}$$

where $\lambda\geq 0$ is a parameter, a, b are positive constants and f reaches the critical growth. We use a scaling iterative algorithm to find numerical solutions to the problem on a large enough bounded domain with several particular nonlinearities f, including those with critical growth. We also study the behavior of the solutions as λ decreases to 0 in consonance with the theoretical study in Part I.

1. Introduction

Part I of the paper deals with the existence of positive solutions for the following nonlinear Kirchhoff-type problem

$$\begin{cases} \left(a+\lambda\int\limits_{\mathbb{R}^3}|\nabla u|^2dx+\lambda b\int\limits_{\mathbb{R}^3}|u|^2dx\right)(-\Delta u+bu)=f(u), \text{ in } \mathbb{R}^3, \\ u\in H^1(\mathbb{R}^3),\ u>0, \text{ in } \mathbb{R}^3, \end{cases} \tag{1.1}$$

where $\lambda\geq 0$, a, b are positive constants and the general nonlinearity f reaches critical growth. The main results in Part I is outlined in the following. Assume the conditions

* Corresponding author.
E-mail address: gucong@math.tamu.edu (C. Gu).

http://dx.doi.org/10.1016/j.jmaa.2017.09.012
0022-247X/

(H_1) $f \in C(\mathbb{R}_+, \mathbb{R}_+)$, $\mathbb{R}_+ = [0, \infty)$ and $\lim_{s \to 0^+} \frac{f(s)}{s} = 0$;

(H_2) $\limsup_{s \to \infty} \frac{f(s)}{s^5} \leq 1$;

(H_3) there exist $k \in (2, 6)$ and $\mu > \mu_k$ such that $f(s) \geq \mu s^{k-1}$ for all $s \geq 0$, where

$$\mu_k = \left[\frac{3(k-2)}{2kS^{\frac{3}{2}}}\right]^{\frac{k-2}{2}} a^{\frac{6-k}{4}} C_k^{\frac{k}{2}}$$

Here, S and C_k are the best constants of Sobolev embeddings $D^{1,2}(\mathbb{R}^3) \hookrightarrow L^6(\mathbb{R}^3)$ and $H^1(\mathbb{R}^3) \hookrightarrow L^k(\mathbb{R}^3)$ respectively, namely,

$$S\left(\int_{\mathbb{R}^3} |u|^6 \, dx\right)^{\frac{1}{3}} \leq \int_{\mathbb{R}^3} |\nabla u|^2 \, dx, \text{ for all } u \in D^{1,2}(\mathbb{R}^3) \tag{1.2}$$

and

$$C_k\left(\int_{\mathbb{R}^3} |u|^k dx\right)^{\frac{2}{k}} \leq \int_{\mathbb{R}^3} \left(|\nabla u|^2 + b|u|^2\right) dx, \text{ for all } u \in H^1(\mathbb{R}^3). \tag{1.3}$$

The following existence theorem is then proved.

Theorem 1.1. *Assume that f satisfies the conditions (H_1)–(H_3). Then there exists a positive constant λ^* such that, for every $\lambda \in (0, \lambda^*)$, problem (1.1) has at least one nontrivial positive solution.*

Also, when $\lambda = 0$ in (1.1), the equation reduces to

$$-a\Delta u + abu = f(u), \text{ in } \mathbb{R}^3. \tag{1.4}$$

The following theorem regarding the asymptotics of the solution to problem (1.1) as $\lambda \to 0$ is proved.

Theorem 1.2. *For every $\lambda > 0$ small enough, there exists a positive solution $u_\lambda \in H^1(\mathbb{R}^3)$ for problem (1.1) such that, u_λ converges to u in $H^1(\mathbb{R}^3)$ as $\lambda \to 0$ along a subsequence, where u is a ground state solution for the limit problem (1.4).*

The goal of part II of the current series is to develop algorithms and find numerical solutions to Kirchhoff type problems. Such studies are rather scarce to the best knowledge of the authors. However, there is extensive literature for numerical algorithms for semi-linear elliptic equations [6,4,3]. For subcritical homogeneous nonlinearities, we are actually able to transform the Kirchhoff type problem, which is a quasi-linear problem, into a scaling of a semi-linear problem. However, in other cases, a direct modification of the algorithm is needed to deal with the extra non-local nonlinearity involved. In either of the cases, we are able to obtain numerical results that agree well with the theory and indicate the sharpness of our conditions.

In practice, we numerically solve the problem on bounded domain instead of on $\mathbb{R}^3$ due to the limitations of our grid-based numerical methods. However, it can be reasonably expected, though not proved, that given a large enough domain, the solution should be a good approximation to that of problem (1.1) for the whole space. In fact, under the conditions in [8], the radially symmetric solution in C^2 demonstrates exponential decay as $|x| \to \infty$, which partially justifies our claim and practice. We consider, namely, the following problem

$$\begin{cases} \left(a+\lambda\|u\|^2\right)(-\Delta u+bu)=f(u), \text{ in } \Omega, \\ u\in H_0^1(\Omega),\ u>0, \text{ in } \Omega, \end{cases} \tag{1.5}$$

where

$$(u,v)=\int_\Omega (\nabla u\cdot\nabla v+buv)\,dx, \quad \|u\|=(u,u)^{\frac{1}{2}}, \quad \lambda\geq 0, \quad a,b>0,$$

and $\Omega\subset\mathbb{R}^3$ is some large enough bounded domain. The main difficulties of such numerical studies are that the solutions could be rich in multiplicity, some of which are hard to capture numerically. Also, trivial iterative methods are prone to either diverge or to converge to zero. To deal with these issues, we adopt ideas from [4,3] to help design algorithms. The "algorithm" is indifferent to the numerical method used to solve the underlying PDE in each iteration step. Two numerical methods are used here. The first is the finite difference method for the one-dimensional radially symmetric formulation ($u=u(r)$). The second is the intrinsically three-dimensional finite volume method implemented with OpenFOAM.

The remainder of the paper is organized as follows. In Section 2, we discuss symmetry and uniqueness of the solutions. In Section 3, we study the problem with cubic nonlinearity that can be obtained by a scaling of the semi-linear problem as a starting point of our numerical study. In Section 4, we extend the algorithm to deal with more general nonlinearities. In Section 5 and 6, we show some numerical examples.

2. Preliminary characterization of the solutions

We first discuss properties of the solutions to problem (1.5) using some well established results. For ease of discussion, we introduce a weaker version of (H_2), namely,

(H_2') $\limsup_{s\to\infty}\frac{f(s)}{s^5}<M$ for some $M>0$.

The next lemma shows that solutions are classical.

Lemma 2.1. *Let Ω be a sufficiently smooth bounded domain in $\mathbb{R}^3$ and $u\in H_0^1(\Omega)$ be a weak solution to problem (1.5). Suppose f satisfies (H_1), (H_2') and is locally Hölder continuous. Then u is a C^2 solution.*

Proof. Let $c=a+\lambda\|u\|^2$. By (1.5), u satisfies

$$c(-\Delta u+bu)=f(u).$$

Then the result is standard (essentially contained in [2]). □

Given a positive solution, which must be in C^2, we can conclude that the solution have to be radially symmetric with a single-peak profile.

Proposition 2.2. *Let Ω be a ball domain in $\mathbb{R}^3$ and u is a positive solution of (1.5). Suppose f satisfies (H_1), (H_2') and is in C^1. Then u is radially symmetric with a single-peak profile.*

Proof. Let $c=a+\lambda\|u\|^2$. By (1.5), u satisfies $c(-\Delta u+bu)=f(u)$ with zero Dirichlet condition and u is in C^2. Direct application of [9, Theorem 1] proves the symmetry. □

In general, we do not have uniqueness results for problem (1.5). In fact, the mountain pass theorem (cf. [1,14]) is applicable to prove that there are infinitely many large energy solutions for certain nonlinearities.

See [13] for the details. However, with subcritical homogeneous nonlinearities, more can be said about the solutions. We consider $1 < p < 5$ and the problem

$$\begin{cases} \left(a + \lambda \|u\|^2\right)(-\Delta u + bu) = u^p, \text{ in } \Omega, \\ u \in H_0^1(\Omega), \ u > 0, \text{ in } \Omega, \end{cases} \tag{2.1}$$

along with the associated limit problem with $\lambda = 0$:

$$\begin{cases} a(-\Delta u + bu) = u^p, \text{ in } \Omega, \\ u \in H_0^1(\Omega), \ u > 0, \text{ in } \Omega. \end{cases} \tag{2.2}$$

Proposition 2.3. *Every positive solution of (2.1) (the case of homogeneous nonlinearity) is a scaling of a positive solution to problem (2.2).*

Proof. Given solution u to problem (2.1), then u/η is a solution to (2.2), where

$$\eta = \left(\frac{a + \lambda \|u\|^2}{a}\right)^{\frac{1}{p-1}}. \quad \square$$

Then we combine the above proposition with uniqueness results of problem (2.2) (cf. [12]). Similar ideas can be found in [11].

Proposition 2.4. *Let Ω be a ball centered at the origin in $\mathbb{R}^3$ and u_0 is the positive solution of (2.2). Then problem (2.1) has as many positive solutions as the algebraic equation for $\eta > 0$,*

$$a + \lambda \|u_0\|^2 \eta^2 = a\eta^{p-1}. \tag{2.3}$$

Proof. By [12], u_0 is unique. In light of Proposition 2.3, suppose $u_\lambda = \eta u_0$, with η being a positive scaling factor, solves (2.1). Direct substitution gives equation (2.3). $\square$

Corollary 2.5. *Assume the conditions of Proposition 2.4. If $3 < p < 5$, then (2.1) has a unique positive solution for all $\lambda \geq 0$.*

Proof. Equation (2.3) can be rewritten as

$$1 = \frac{a\eta^{p-1}}{a + \lambda \|u_0\|^2 \eta^2} =: P(\eta). \tag{2.4}$$

Then the function $P(\eta)$ is strictly increasing and continuous. It also attains all positive real numbers. Therefore (2.3) has a unique solution. $\square$

Corollary 2.6. *Assume the conditions of Proposition 2.4. If $p = 3$, then (2.1) has a positive solution if and only if $\lambda < \lambda_{\max} := a/\|u_0\|^2$ and the solution is uniquely determined by ηu_0, where*

$$\eta = \left(\frac{a}{a - \lambda \|u_0\|^2}\right)^{\frac{1}{2}}. \tag{2.5}$$

Proof. It is straightforward to check that (2.3) has a unique positive solution if and only if $\lambda < a/\|u_0\|^2$ and the solution is (2.5). $\square$

Corollary 2.7. *Assume the conditions of Proposition 2.4. If $1 < p < 3$, then (2.1) has a positive solution if and only if*

$$\lambda \le \lambda_{\max} := \frac{a(p-1)(3-p)^{\frac{3-p}{p-1}}}{2^{\frac{2}{p-1}}\|u_0\|^2}. \tag{2.6}$$

If $\lambda = \lambda_{\max}$, then there is a unique solution. If $0 < \lambda < \lambda_{\max}$, then there are exactly two solutions.

Proof. The function $P(\eta)$ defined in (2.4) is differentiable and has a unique critical number. Also

$$\lim_{\eta\to 0^+} P(\eta) = \lim_{\eta\to\infty} P(\eta) = 0.$$

Therefore (2.4) (or equivalently (2.3)) has a unique solution if $\max_{\eta>0} P(\eta) = 1$, has exactly two solutions if $\max_{\eta>0} P(\eta) > 1$, and has no solution if $\max_{\eta>0} P(\eta) < 1$. Direction calculation of the inequality $\max_{\eta>0} P(\eta) \ge 1$ gives the condition (2.6). □

Remark 2.8. Although the uniqueness of solutions to (2.2) is lost on certain domains, such as dumbbell shaped ones, there is a long standing conjecture that the solution is unique on all bounded and convex domains [7]. Uniqueness is proved for domains other than balls under various conditions, for example, in [10]. Therefore, there are chances that the domain shape constraint in Proposition 2.4 can be relaxed.

3. Scaling solution for cubic nonlinearity

First consider numerical study of a special but important case of the cubic nonlinearity $f(s) = s^3$. Proposition 2.3 and Corollary 2.6 give a good characterization of the solution. Moreover, the solution can be expressed explicitly as $u_\lambda = \eta u_0$, where u_0 is the solution of (2.2) (the problem with $\lambda = 0$), and η is given by (2.5). One extra thing we know from the scaling formula is the following asymptotic behavior.

$$\|u_\lambda - u_0\| = O(\lambda), \text{ as } \lambda \to 0^+, \tag{3.1}$$

$$\|u_\lambda\| \propto (\lambda_{\max} - \lambda)^{-\frac{1}{2}} \tag{3.2}$$

Now we move on to the solution algorithm. The Scaling Iterative Algorithm (SIA), which is shown in [4] to be effective in computing (2.2), can be employed. An adapted version of it goes as the following.

Algorithm 3.1 *(SIA).*

1. *Give initial guess $v_0 \ge 0$, $v_0 \not\equiv 0$;*
2. *Find β_{n+1} and v_{n+1} such that*

$$\begin{cases} a\beta_{n+1}(-\Delta v_{n+1} + b v_{n+1}) = v_n^p \text{ in } \Omega, \\ v_{n+1} = 0 \text{ on } \partial\Omega, \\ \|v_{n+1}\| = 1. \end{cases} \tag{3.3}$$

3. *If $\|v_{n+1} - v_n\| > \varepsilon$, repeat Step 2. Otherwise, for $p = 3$ and $\lambda < a\beta_{n+1}$, output ηv_{n+1} with*

$$\eta^2 = \frac{a}{a\beta_{n+1} - \lambda}. \tag{3.4}$$

Problem (3.3) is solved, in practice, by finding w_{n+1} such that

$$\begin{cases} a\left(-\Delta w_{n+1} + b w_{n+1}\right) = v_n^p \text{ in } \Omega, \\ w_{n+1} = 0 \text{ on } \partial\Omega, \end{cases} \tag{3.5}$$

and a subsequent scaling $v_{n+1} = w_{n+1}/\beta_{n+1}$, where $\beta_{n+1} = \|w_{n+1}\|$.

Remark 3.2. The purpose of the condition $\|v_{n+1}\| = 1$ is to keep v_{n+1} globally away from zero/infinity. In practice, $\|v_{n+1}\|_{L^\infty} = 1$, or even $v_{n+1}(x_0) = 1$ can be used instead for the same purpose. These were employed in [4] to reduce computational cost and to gain more control over the location of the peak.

The following theorem shows the effectiveness of the algorithm.

Theorem 3.3. *Let Ω be a sufficiently smooth bounded domain in $\mathbb{R}^3$ and (v_n, β_n) be the sequence generated by Algorithm 3.1 with the initial guess v_0 smooth enough.*

(i) *If $\liminf_{n\to\infty} \|v_n\|_4 > 0$, then there is subsequence of (v_n, β_n), still denote as (v_n, β_n), converging strongly in $H_0^1(\Omega) \times (0, \infty)$;*
(ii) *If the algorithm converges to (v, β) and $\lambda < a\beta$, then a scaling of v, namely $\sqrt{a/(a\beta - \lambda)}\, v$, is a non-trivial classical solution to problem (2.1) (with $p = 3$).*

Proof. Let S be the coefficient of Sobolev embedding defined in (1.2), but for domain Ω instead of $\mathbb{R}^3$. Since $\{w_n\}$ is bounded in $H^1(\Omega)$, namely,

$$a\|w_{n+1}\| \le \|v_n^3\|_2 = \|v_n\|_6^3 \le \frac{1}{S^3}\|v_n\|^3 = \frac{1}{S^3}.$$

They are also bounded by the $H^2(\Omega)$-estimate of equation (3.5). Then by the Sobolev embedding theorem, $\{w_n\}$ has a subsequence (still denoted as $\{w_n\}$) converging to w in $W^{1,q}(\Omega)$ for any $q < 6$. Equation (3.5) also gives

$$c\|v_n\|_4^4 = a\left(w_{n+1}, v_n\right) \le a\|w_{n+1}\|\|v_n\| = a\|w_{n+1}\|.$$

The condition $\liminf_{n\to\infty} \|v_n\|_4 > 0$ ensures that $\beta_n = \|w_{n+1}\|$ is bounded away from 0. Hence $\beta_n \to \beta > 0$ and $v_n = w_n/\beta_n$ converges to $v = w/\beta$ in $W^{1,q}(\Omega)$. This completes the proof of part one.

If the algorithm converges, it is obvious that the limit pair (v, β) is a non-trivial solution to $a\beta\left(-\Delta v + bv\right) = v^3$. Notice that $\beta^{-\frac{1}{2}} v$ is a solution to problem (2.2). The second part of the theorem is a direct result from Corollary 2.6 above. The solution is classical by Lemma 2.1. □

Remark 3.4. There are several possible ways this algorithm could fail to work. First, there is a possibility that $\liminf_{n\to\infty} \|v_n\|_4 = 0$. Second, there is an essential gap between the first and the second part of the above theorem. For example, the iteration may oscillate between several functions, none of which are solutions of the problem.

The purpose of studying the cubic nonlinearity is that a solution can be obtained by directly scaling from an analytically and numerically well studied problem, namely (2.2). A lot of information is available including the uniqueness of such a scaled solution and the bounds and asymptotic behavior as λ changes. This gives a perfect entry point for studying Kirchhoff-type problems and provides benchmark cases for later introduced algorithms.

4. Implicit scaling iterative algorithm

Algorithm 3.1 is not directly applicable to other kinds of nonlinearities, especially those more general ones satisfying (H_1)–(H_3), which is the main interest in this series. In this section, we shift our attention back to the more general problem (1.5). One way to deal with this problem is to use algorithms designed based on the variational structure, in our case, the functional

$$\Phi_\lambda(u) = \frac{a}{2}\|u\|^2 + \frac{\lambda}{4}\|u\|^4 - \int_\Omega F(u)\,dx, \tag{4.1}$$

and $F(t) = \int_0^t f(s)\,ds$. This includes algorithms such as the Mountain-Pass Algorithm [6,4] and the Optimal Scaling Algorithm [3]. Although being able to utilize available variational structure is generally preferable, we take a different approach here, which is applicable to problems even without a variational structure.

We start by observing that the success of ISA partially lies in the fact that the "shape" and the "size" of the iterative solutions are treated separately, which breaks the unstable feedback that drives the iterations to infinity/zero in "size". While given any function $v \in H_0^1(\Omega)$, one can easily find the "size" — $\|v\|$, and the "shape" — $v/\|v\|$, it is not always clear how one can determine the appropriate "size" when only given the "shape" of the function. One specially good situation is the cubic nonlinearity discussed in Section 3. Not only do we have an explicit formula for the "size" η, but we also just need to do it once at the very end, which is a rare occurrence. Heuristically, if we try to find the size η_{n+1} at every iteration using equation (3.4), namely,

$$\eta_{n+1}^2 = \frac{a}{a\beta_{n+1} - \lambda},$$

and eliminate β_{n+1} in problem (3.3), we get our new problem in each iteration, that is, to find the new "shape" — v_{n+1} and "size" — η_{n+1} satisfying

$$\begin{cases} -\Delta v_{n+1} + b v_{n+1} = g(\eta_{n+1}, v_n) \text{ in } \Omega, \\ v_{n+1} = 0 \text{ on } \partial\Omega, \\ \|v_{n+1}\| = 1, \end{cases} \tag{4.2}$$

where $g \in C(\mathbb{R}_+^2, \mathbb{R}_+)$ is defined by

$$g(\eta_{n+1}, v_n) = \frac{v_n^3 \eta_{n+1}^2}{a + \lambda \eta_{n+1}^2}.$$

The old "shape" — v_n is known at the beginning of each iteration. The continuity of g in variable η_{n+1} suggests a continuous dependency of v_{n+1} on the choice of η_{n+1}. Therefore, we can solve problem (4.2) by adjusting η_{n+1} until $\|v_{n+1}\| = 1$ is attained. This way of searching for η_{n+1} such that $\|v_{n+1}\| = 1$ is what makes this method an implicit version of the scaling iterative algorithm (ISIA). It maintains some of the desired benefits of SIA, while being easily extendable to a wider range of problems.

From now on, we focus on our main interest, problem (1.5) generally under similar condition as (H_1)–(H_3) on f. The algorithm goes as the following.

Algorithm 4.1 *(ISIA).*

1. *Give initial guess* $v_0 \geq 0$, $\|v_0\| = 1$;

2. *Find* η_{n+1} *and* v_{n+1} *such that*

$$\begin{cases} -\Delta v_{n+1} + b v_{n+1} = g(\eta_{n+1}, v_n) \text{ in } \Omega, \\ v_{n+1} = 0 \text{ on } \partial\Omega, \\ \|v_{n+1}\| = 1, \end{cases} \tag{4.3}$$

where $g : \mathbb{R}_+^2 \to \mathbb{R}_+$ *is defined by*

$$g(\eta, s) = \frac{f(\eta s)}{\eta\,(a + \lambda\eta^2)}. \tag{4.4}$$

3. *If* $\|v_{n+1} - v_n\| > \varepsilon$, *repeat Step 2. Otherwise, output* $\eta_{n+1} v_{n+1}$.

Problem (4.3) is solved by an inner iteration on η. For each choice of η, we can find w satisfying

$$\begin{cases} -\Delta w + b w = g(\eta, v_n) \text{ in } \Omega, \\ w = 0 \text{ on } \partial\Omega. \end{cases} \tag{4.5}$$

We then show the mapping $\eta \mapsto w$ as defined by the above problem is continuous, and under certain conditions, is able to attain w with H^1-norm of unity. Therefore, problem (4.3) can be solved with any general algorithm for continuous problems, such as the *bisection algorithm*, within each iteration of ISIA.

Lemma 4.2. *Assume that* f *satisfies* (H_1). *If* $v_n \in L^\infty(\Omega)$ *and* $v_n \not\equiv 0$, *then the mapping* $\eta \mapsto w$ *defined by problem* (4.5) *is in* $C\left(\mathbb{R}_+, H_0^1(\Omega)\right)$.

Proof. Let $\tilde{g}_\eta$ be the function defined by $x \mapsto g(\eta, v_n(x))$ for all $x \in \Omega$. Given arbitrary but fixed $\eta \geq 0$ and a sequence $\eta_m \to \eta$, by continuity of f, $\tilde{g}_{\eta_m}$ converges pointwise to $\tilde{g}_\eta$. On the other hand, f is continuous on the closed interval $[0, M]$, for some $M > (\max\{\eta_m\})\,\|v_n\|_{L^\infty}$. Therefore f is bounded on $[0, M]$, and hence $\{\tilde{g}_{\eta_m}\}$ is uniformly bounded if the limit $\eta > 0$. When $\eta = 0$, the same can be claimed using the fact that $\lim_{s\to 0^+} f(s)/s = 0$. In either case, since Ω is bounded, we conclude that $\tilde{g}_{\eta_m} \to \tilde{g}_\eta$ in $L^2(\Omega)$ by dominated convergence theorem. Finally, by continuity of the inverse of the elliptic operator, the proof is complete. □

We introduce the condition (H_2') and (H_3') as weaker versions of (H_2) and (H_3) respectively.

(H_2') $\limsup_{s\to\infty} \dfrac{f(s)}{s^5} < M$ for some $M > 0$;
(H_3') there exists a $k \in (2, 6)$ and $\mu > 0$ such that $f(s) \geq \mu s^{k-1}$ for all $s \geq 0$.

Lemma 4.3. *If* f *satisfies* (H_1) *and* (H_3'), $\|v_n\| = 1$, $v_n \in L^\infty(\Omega)$ *and* λ *is sufficiently small, then there exists an* η *such that the solution* w *in problem* (4.5) *has* H^1*-norm of unity. If* $k < 4$ *in* (H_3'), *then* η *can be chosen such that* $\eta < \sqrt{a(k-2)/\lambda(4-k)}$.

Proof. First, if $\eta \to 0$, then by the same argument as in Lemma 4.2, we have $\|w\| = 0$. On the other hand, problem (4.5) and (H_3') gives the following estimate,

$$\|w\| = \|w\|\|v_n\| \geq (w, v_n) \geq \int_\Omega \frac{\mu(\eta v_n)^{k-1} v_n}{\eta(a + \lambda\eta^2)}\,dx = \frac{\mu\|v_n\|_k^k \eta^{k-2}}{a + \lambda\eta^2} =: P(\eta), \tag{4.6}$$

where μ and k are from condition (H_3'). **Case 1:** $k > 4$. $P(\eta)$ can be made arbitrarily large by choosing sufficiently large η. **Case 2:** $k = 4$. As $\eta \to \infty$, $P(\eta) \to \mu\|v_n\|_k^k/\lambda$. Therefore, if

$$\lambda < \mu\|v_n\|_k^k,$$

then we have $P(\eta) > 1$ whenever η is sufficiently large. **Case 3:** $k < 4$. The maximum of $P(\eta)$ is achieved at the maximizer $\eta^* = \sqrt{a(k-2)/\lambda(4-k)}$ and the maximum value is given by

$$\max_{\eta>0} P(\eta) = P(\eta^*) = \frac{(4-k)\mu\|v_n\|_k^k}{2a}\left[\frac{a(k-2)}{\lambda(4-k)}\right]^{\frac{k-2}{2}}.$$

Similar to the situation in case 2, if

$$\lambda < \left[\frac{(4-k)\mu\|v_n\|_k^k}{2a}\right]^{\frac{2}{k-2}} \frac{a(k-2)}{4-k},$$

then we can make $P(\eta^*) > 1$. In all of the three cases $\sup_{\eta>0} P(\eta) > 1$, given sufficiently small λ. By Lemma 4.2 and the intermediate value theorem, the proof is complete. □

Lemma 4.2 and 4.3 guarantee the solvability of problem (4.3) using the bisection algorithm in each iteration. The following lemma deals with the trend of $\{\eta_n\}$.

Lemma 4.4. *Assume that f satisfies (H_1), (H_2') and (H_3'). Let (v_n, η_n) be the sequence generated by Algorithm 4.1 with the initial guess v_0 smooth enough. If $\liminf_{n\to\infty} \|v_n\|_k > 0$ and λ is sufficiently small, then $\{\eta_n\}$ is bounded away from both infinity and zero.*

Proof. By (H_1) and (H_2'), for any $\varepsilon > 0$, there exists an $M_\varepsilon > 0$ such that

$$f(s) < \varepsilon s + M_\varepsilon s^5.$$

An estimate on (4.3) and the Sobolev embedding gives

$$1 = \|v_{n+1}\|^2 \le \int_\Omega \frac{\left(\varepsilon\eta_{n+1}v_n + M_\varepsilon\eta_{n+1}^5 v_n^5\right) v_{n+1}}{\eta_{n+1}\left(a + \lambda\eta_{n+1}^2\right)}\, dx \le \frac{\varepsilon + M_\varepsilon\eta_{n+1}^4}{a + \lambda\eta_{n+1}^2}$$

Choosing $\varepsilon < a$ reveals that η_{n+1} is bounded away from zero.

To show that $\{\eta_n\}$ is also bounded above, we look at estimate (4.6), but replacing w with v_{n+1} and η with η_{n+1},

$$1 \ge \frac{\mu\|v_n\|_k^k \eta_{n+1}^{k-2}}{a + \lambda\eta_{n+1}^2}.$$

Case 1: $k > 4$. It is obvious that η_{n+1} has to be bounded. **Case 2:** $k = 4$. Recall that $\lambda < \inf_n \mu\|v_n\|_k^k$ from Lemma 4.3. It is obvious. **Case 3:** $k < 4$. It is guaranteed by the last statement of Lemma 4.3. □

Here we have an analogy to Theorem 3.3.

Theorem 4.5. *Let Ω be a sufficiently smooth bounded domain in $\mathbb{R}^3$. Assume that f satisfies (H_1), (H_2') and (H_3') and λ is sufficiently small. Let (v_n, η_n) be the sequence generated by Algorithm 4.1 with the initial guess v_0 smooth enough.*

(i) *If* $\liminf_{n\to\infty}\|v_n\|_k > 0$ *and* f *is subcritical (i.e.,* $\limsup_{s\to\infty} f(s)/s^q < M$ *for some* $q < 5$ *and* $M > 0$*), then there is a subsequence of* (v_n, η_n)*, still denote as* (v_n, η_n)*, converging strongly in* $H_0^1(\Omega)\times(0,\infty)$*;*
(ii) *If the algorithm converges to* (v, η)*, then* ηv *is a non-trivial solution to problem (1.5).*

Proof. Let $\tilde{g}_n$ be the function defined by $x \mapsto g(\eta_{n+1}, v_n(x))$ for all $x \in \Omega$. Since f is subcritical, $\{\eta_n\}$ is bounded and $\|v_n\| = 1$, we have that $\{\tilde{g}_n\}$ is bounded in $L^{6/q}(\Omega)$, and hence $\{v_n\}$ is bounded in $W^{2,6/q}(\Omega)$ by elliptic estimates. Therefore, there is a subsequence of v_n converging strongly to v in $H_0^1(\Omega)$. Also, since $\{\eta_n\}$ is bounded away from zero and away from infinity, there is a subsequence $\eta_n \to \eta > 0$. This proves the first part.

For the second part, by the convergence, the limit pair (v, η) satisfies

$$\eta(a + \lambda\eta^2)(-\Delta v + bv) = f(\eta v),$$

and $\|v\| = 1$. Therefore ηv is clearly a solution to problem (1.5). □

In the case of critical nonlinearity, the conditions are not enough to prove convergence of a subsequence due to the lack of compactness. As is shown in Part I, such problems are more delicate. In fact, the numerical investigations in the following section show that problem (1.5) with critical nonlinearity is substantially dependent on (H_3) itself, while the weakened version (H_3') will not work. This is very different from the case of subcritical nonlinearity. Apart from that, this new algorithm suffers the same problem outlined in Remark 3.4, i.e., convergence is not guaranteed.

5. Numerical experiments

In this section, we provide some numerical examples using the Algorithms 3.1 and 4.1 detailed in the previous sections.

The algorithm itself is indifferent to the numerical methods used to solve the linear problem (4.5). In light of Proposition 2.2, the most efficient way is probably to use the one-dimensional radially symmetric formulation of the problem in $w = w(r)$, namely,

$$\begin{cases} -\dfrac{1}{r^2}\dfrac{\partial}{\partial r}\left(r^2\dfrac{\partial w}{\partial r}\right) + bw = g \quad \text{on } r \in (0, R), \\ \dfrac{\partial w}{\partial r} = 0 \text{ at } r = 0, \quad w = 0 \text{ at } r = R. \end{cases}$$

We then use the finite difference approximation to the above problem, for example,

$$-\frac{1}{r_j^2}\left(r_{j+\frac{1}{2}}^2\frac{w_{j+1}-w_j}{h} - r_{j-\frac{1}{2}}^2\frac{w_j - w_{j-1}}{h}\right)\frac{1}{h} + bw_j = g_j.$$

There is no stencil point placed at $r = 0$. The solution value at $r = 0$ is obtained through extrapolation.

Although the above symmetric formulation is sufficient in dealing with the problem at hand, we also want to explore intrinsically three-dimensional solver for non-spherical domains and also for future extension to symmetry-breaking problems. The OpenFOAM library, which implements the finite volume method on three dimensional unstructured meshes, is used as another tool to solve equation (4.5). OpenFOAM is highly useful due to its equation-mimicking capabilities and easy implementation of solvers for PDEs on three dimensional domain. More information on OpenFOAM can be found in [5]. In the following examples, the problems are solved on three kinds of meshes. The first kind is spherical mesh based on a direct tessellation of the spherical coordinates. The second kind is hexahedron-dominant cubic mesh with tiered

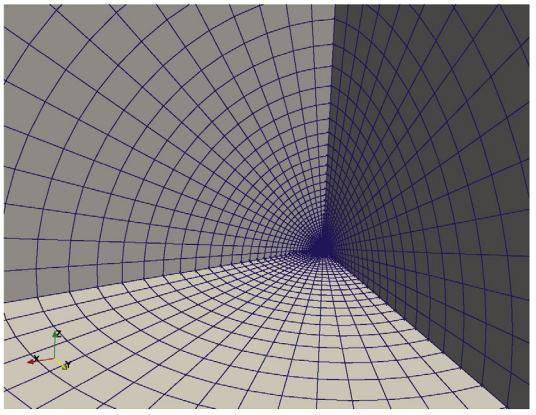

(a) Spherical mesh (S-mesh)

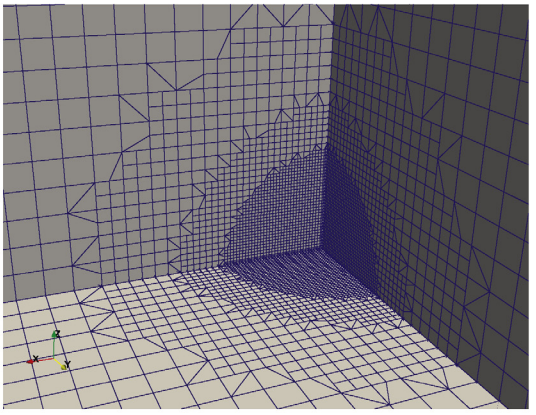

(b) Tiered Cubic mesh (TC-mesh)

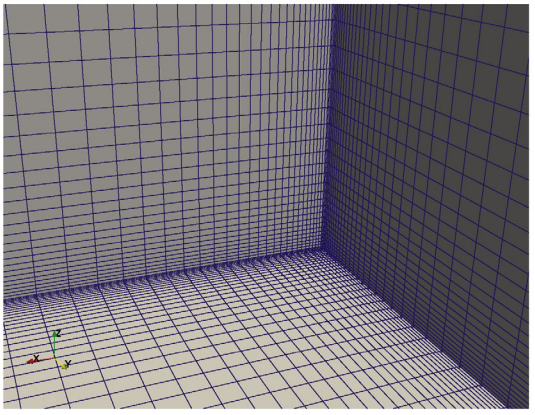

(c) Graded Cubic mesh (GC-mesh)

Fig. 1. Comparison of cross-sections near the center of three kinds of meshes.

refinement regions. The center region consists of uniform fine cubes and the transition between different refinement tiers are made up of tetrahedrons. The third kind is orthogonal hexahedral mesh with size grading toward the center with the choice of different grading ratios. See Fig. 1 for a comparison of the mesh cross-sections.

The domain Ω is typically chosen to be either the cube $C_R = (-R, R)^3$ or the ball $B_R = \{x : |x| < R\}$. We want to find sufficiently large domains in order that the numerical solutions are not affected by further enlargement of the domain in the numerical studies.

To visualize the solutions that are three dimensional, we either find a cross-section or a line and draw the profile of the solutions on the section or along the line.

Example 5.1 *(Cubic nonlinearity $f(s) = s^3$).* We consider Problem (2.1) ($p = 3$). In all tests we have done, the algorithms ISA and ISIA produce exactly the same result because they are equivalent as outlined in Section 4. Therefore the following data are for both of the algorithms. We choose $\lambda = 0.005$, safely away from the $\lambda_{\max}$, which is around 0.0133 for all meshes considered.

This example serves to compare and cross-verify all the numerical practices employed. To reduce redundancy, we only list in Table 1 some properties of the solutions, namely the peak value and the H^1-norm, to briefly indicate how similar the results obtained using different numerical approaches are. Solution profiles, either on a cross-section or on the r-axis/x-axis, are visualized in Fig. 2. The first group in Table 1 is intended to show that the solutions are the same if we keep the mesh density and enlarge the domain. As a result, the domain B_{10} is considered "large enough" to approximate whole space problems for all practical

Table 1
Solutions overview for cubic nonlinearity ($a = 1$, $b = 1$, $\lambda = 0.005$).

Domain	Mesh	Cells	Peak	H^1-norm	$\lambda_{\max}$
B_{10}	Radial	1k	5.49734	11.02337	0.01323
B_{50}	Radial	5k	5.49734	11.02337	0.01323
B_{100}	Radial	10k	5.49734	11.02337	0.01323
B_{10}	Radial	1k	5.49734	11.02337	0.01323
B_{10}	Radial	5k	5.49925	11.02338	0.01323
B_{10}	Radial	10k	5.49934	11.02338	0.01323
B_{10}	Radial	300	5.48751	11.02320	0.01323
B_{10}	S-mesh	99k	5.47777	10.96470	0.01332
C_{10}	TC-mesh	255k	5.47679	10.99736	0.01327
C_{10}	GC-mesh	274k	5.47491	10.97465	0.01330

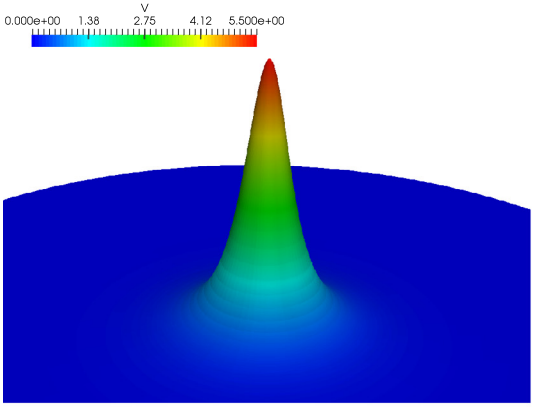

(a) Values on cross-section for S-mesh.

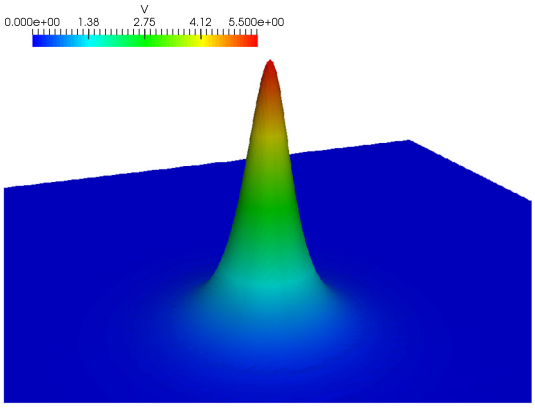

(b) Values on cross-section for TC-mesh.

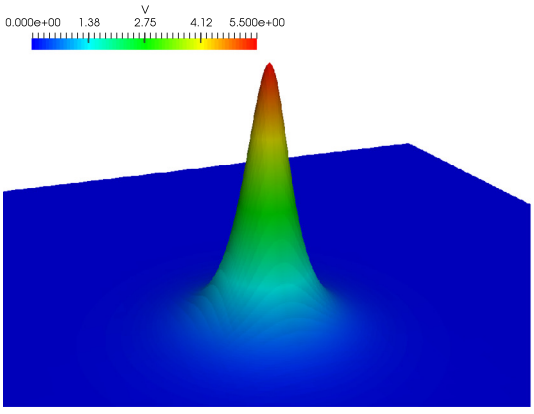

(c) Values on cross-section for GC-mesh.

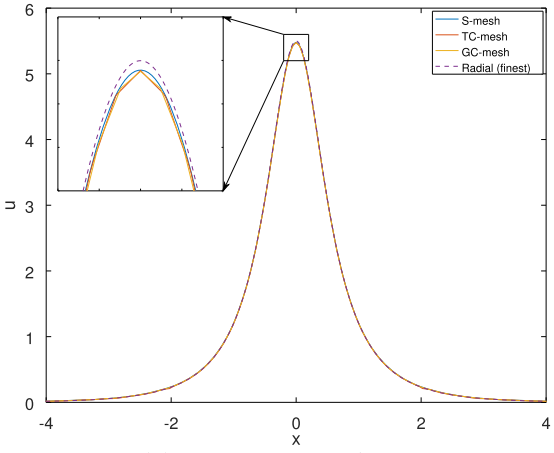

(d) Values on r-axis/x-axis.

Fig. 2. Visualization and comparison of solutions on different meshes for cubic nonlinearity ($a = 1$, $b = 1$, $\lambda = 0.005$).

purposes. The second group in Table 1 is intended to show the trend of convergence when we refine the mesh on a fixed domain B_{10}. The third group in Table 1 is intended to compare the radially symmetric solver (denoted by "Radial" in the mesh column) with the intrinsically three-dimensional OpenFOAM solver under several mesh configurations, namely those illustrated in Fig. 1. It can be observed that the numerical solutions are reasonably close to each other despite vastly different numerical approach, domain and mesh structure.

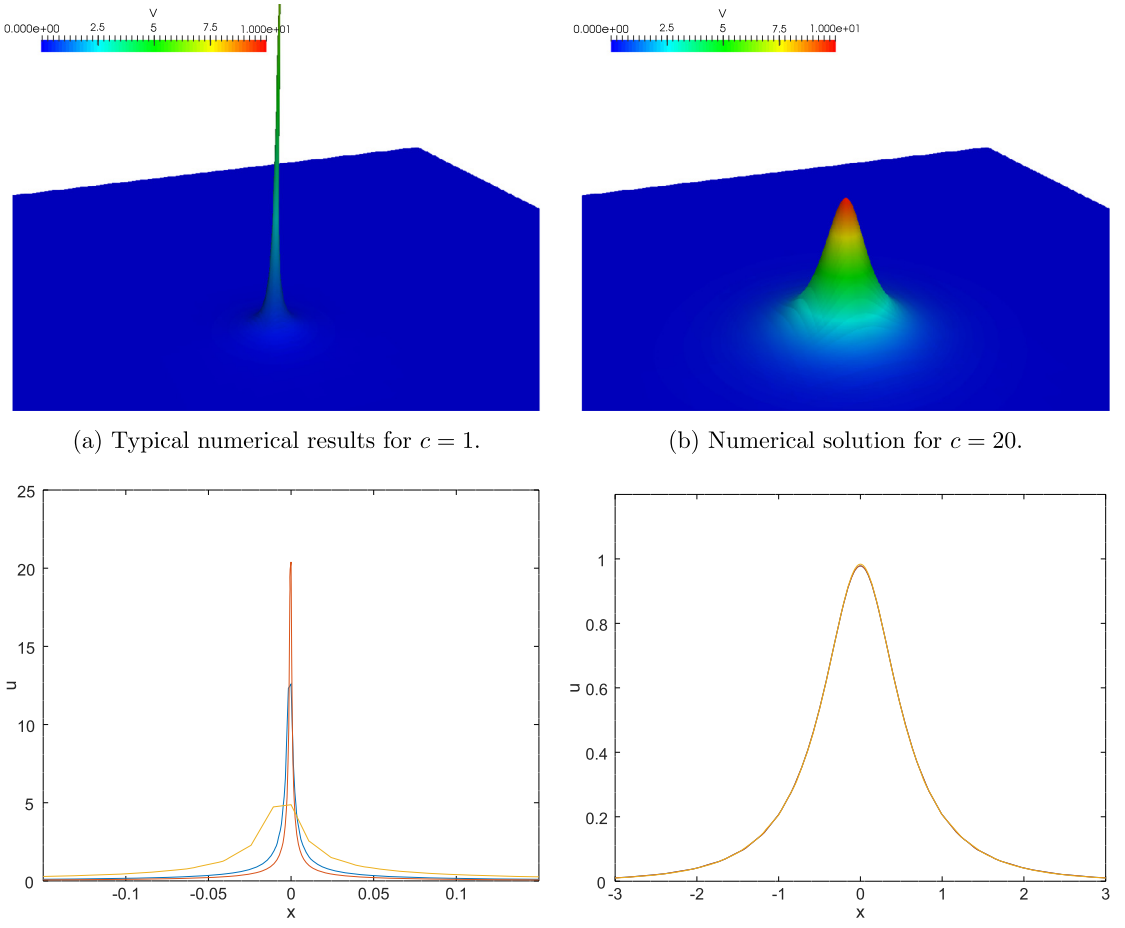

(a) Typical numerical results for $c = 1$.

(b) Numerical solution for $c = 20$.

(c) Peak growth for $c = 1$.

(d) Numerical solution for $c = 20$.

Fig. 3. Comparison of numerical results for $c = 1$ and $c = 20$ (as in $f(s) = cs^3 + s^5$) ($a = 1$, $b = 1$, $\lambda = 0.001$).

Although in ISIA, we don't know the bound for λ a priori, because ISIA produce exactly the same solution as ISA, they share the same upper limit of λ and behavior as $\lambda \to 0^+$ and as $\lambda \to \lambda_{\max}^-$ found in (3.1) and (3.2).

Example 5.2 *(Critical nonlinearity $f(s) = cs^3 + s^5$).* As seen from Theorem 4.5, there is not much difference between condition (H_3) and (H_3') if the nonlinearity is subcritical. That's why the above example doesn't technically satisfy (H_3) but is still perfectly fine. However, we find that conditions like (H_3) is crucial when we study the critical nonlinearity numerically.

Choosing $c = 20$ ensures that (H_3) is satisfied with $k = 4$, while choosing $c = 1$ fails the condition. Visualizations of the numerical results can be found in Fig. 3. We also put out an overview of the numerical results in Table 2. The GC-mesh configurations used are different in their resolution near the center through adjustment of the grading ratio (the ratio between the sizes of the finest cell and the coarsest cell). In the case of $c = 1$, the iterations seem to converge for any particular mesh configuration. But a serious problem emerges when we look at the converged results across different meshes: there are vast discrepancies. This is a clear violation of "mesh convergence", a prerequisite for the validity of any claimed numerical solutions. These numerical results are thus pseudo solutions specific for each mesh configuration. In contrast, when $c = 20$, the numerical results are essentially the same across all mesh configurations. To be precise, the situation here doesn't entirely rule out the possibility of existence of a solution without (H_3), but rather, there is a fundamental change in problem (1.5) that keep our algorithm from producing a mesh convergent

Table 2
Solutions overview for nonlinearity $f(s) = cs^3 + s^5$ ($a = 1$, $b = 1$, $\lambda = 0.001$).

Domain	Mesh	Cells	$c = 1$		$c = 20$	
			Peak	H^1-norm	Peak	H^1-norm
B_{10}	Radial	1k	15.8924	3.42986	0.98041	1.92669
B_{10}	Radial	5k	35.4826	3.42105	0.98077	1.92669
B_{10}	Radial	10k	28.2615	3.59976	0.98078	1.92669
C_{10}	GC (ratio=20)	1m	13.4778	2.03297	0.98380	1.91298
C_{10}	GC (ratio=1000)	512k	34.7059	2.02867	0.97826	1.91827
C_{10}	GC (ratio=3000)	512k	56.1766	2.03089	0.97741	1.91563

Table 3
Selected mesh-convergent numerical solutions for c values (as in $f(s) = cs^3 + s^5$) not meeting the requirement of (H_3) ($a = 1$, $b = 1$, $\lambda = 0.001$, computed on B_{10} domain with radial mesh of 10k cells).

c	Peak	H^1-norm
2.5	4.99268	3.63561
3	3.79272	3.62144

Table 4
Asymptotic behavior as $\lambda \to 0^+$ ($a = 1$, $b = 1$, $c = 20$, computed on B_{10} domain with radial mesh of 10k cells).

λ	Peak	H^1-norm	$\|u_\lambda - u_0\|$	Order
0	0.97893	1.92320		
1×10^{-5}	0.97895	1.92324	3.4838×10^{-5}	
1×10^{-4}	0.97912	1.92335	3.4847×10^{-4}	1.0001
1×10^{-3}	0.98078	1.92669	3.4930×10^{-3}	1.0010

Table 5
Asymptotic behavior as $\lambda \to \infty$ ($a = 1$, $b = 1$, $c = 20$, computed on B_{10} domain with radial mesh of 10k cells).

λ	Peak	H^1-norm	Order
1	5.41312×10^{1}	1.16970×10^{1}	
10	1.72300×10^{2}	3.71354×10^{1}	0.50171
100	5.45379×10^{2}	1.17516×10^{2}	0.50031
1000	1.72481×10^{3}	3.71647×10^{2}	0.50003

result if c is too small, just as suggested by (H_3). This is a good indication of what role condition (H_3) could play for critical nonlinearities.

In fact, our numerical investigation shows that mesh-convergent solutions are likely to be found for $c \geq 2.5$ in $f(s) = cs^3 + c^5$. This is a little weaker than the bound derived from (H_3), which is around 4. This might inspire analysts to come up with even sharper conditions than (H_3). Some such solutions are described in Table 3.

Another interesting topic is the trend as λ changes. We don't know yet the asymptotic behavior as $\lambda \to 0^+$ other than in the case of cubic nonlinearity, which is of the first order given by (3.1). Table 4 shows that the convergence as $\lambda \to 0^+$ for $f(s) = cs^3 + s^5$ is also exactly of the first order. On the other hand, when λ is large, no upper limit is imposed by the algorithm in the case of $k > 4$ in (H_3). We can indeed find solutions for larger λ and the H^1-norm of the solutions grow in proportion to $\sqrt{\lambda}$, as shown in Table 5.

Table 6
Multiple solutions for quadratic nonlinearity ($a = 1$, $b = 1$, $\lambda = 5 \times 10^{-4}$, computed on B_{10} domain with radial mesh of 10k cells).

Solution No. 1		Solution No. 2		$\lambda_{\max}$
Peak	H^1-norm	Peak	H^1-norm	
4.96017	19.15427	27.03929	104.41538	9.54341×10^{-4}

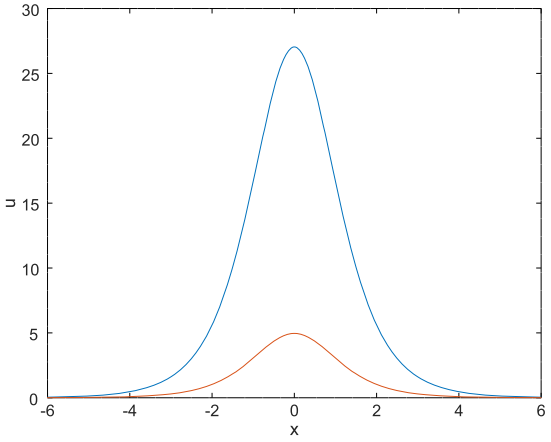

Fig. 4. Multiple solutions for quadratic nonlinearity along r-axis ($a = 1$, $b = 1$, $\lambda = 5 \times 10^{-4}$, computed on B_{10} domain with radial mesh of 10k cells).

6. An example with multiple solutions

Corollary 2.7 describes a situation when there are two solutions to problem (2.1). Here we give an example as $p = 2$ (quadratic nonlinearity). Algorithm 3.1 is used except that the output value in Step 3 is now different. In particular, when $p = 2$, equation (2.3) become a simple quadratic equation, whose solutions are

$$\eta_1, \eta_2 = \frac{a \pm \left(a^2 - 4a\lambda\|u_0\|^2\right)^{\frac{1}{2}}}{2\lambda\|u_0\|^2}, \text{ if } \lambda < \lambda_{\max} = \frac{a}{4\|u_0\|^2}$$

Noticing the fact that $u_0 = v/\beta$, where (v, β) is the converged pair, we can write η and $\lambda_{\max}$ in terms of β instead as

$$\eta_1, \eta_2 = \frac{a\beta^2 \pm \left(a^2\beta^4 - 4a\lambda\beta^2\right)^{\frac{1}{2}}}{2\lambda}, \text{ if } \lambda < \lambda_{\max} = \frac{a\beta^2}{4}$$

A numerical example is shown in Table 6 and Fig. 4.

7. Conclusion and future research

In order to use numerical methods to gain more insights into the Kirchhoff type problems (1.1), we first characterize the solutions using some well established results. This gives us the idea of what we can expect when we are trying to find numerical solutions. Then we adapt the scaling iterative algorithm to deal with the Kirchhoff type problem. The new algorithm is called Implicit Scaling Iterative Algorithm (ISIA). Although convergence is not guaranteed mathematically, it has its own benefits. For example, there is no direct dependence on the variational structure of the problem, which makes it more widely applicable. In practice, this algorithm works well and efficiently in dealing with the Kirchhoff type problem.

We've verified the new algorithm, ISIA, with cubic nonlinearity. We have also confirmed that there is little difference in spherical and cubic domains as long as the domains are sufficiently large to approximate the whole space problem. And then we've successfully found numerical solutions for critical nonlinearity $f(s) = cs^3 + c^5$. It has been clearly shown that condition (H_3) play some substantial role here. We can also see very clear asymptotic behavior as $\lambda \to 0^+$ and $\lambda \to \infty$.

Despite the success in finding numerical solutions for the Kirchhoff type problem involing critical growth, there are many issues yet to be explored. First, it will be beneficial to extend existing algorithms developed for semi-linear elliptic equation that directly utilize the variational structures, such as the mountain pass algorithm. Better convergence properties can be expected with the extra information used in these algorithms. Second, more numerical experiments can be done to find sharper conditions and motivate future development of the theories. Third, multiplicity results are not known in many situations. If new numerical techniques can be developed to capture multiple solutions for such quasi-linear problems, new horizons will open for analysts and numerical investigators alike.

Acknowledgments

This research was partially supported by the Fundamental Research Funds for the Central Universities 2015XKMS072 and by Qatar National Research Fund project #NPRP 9-166-1-031 and by the National Center for Theoretical Sciences (NCTS) and Ministry of Science and Technology (MOST) grant 103-2115-M-002-005 of Taiwan.

References

[1] T. Bartsch, Infinitely many solutions of a symmetric Dirichlet problem, Nonlinear Anal. 20 (10) (1993) 1205–1216.
[2] H. Brezis, T. Kato, Remarks on the Schrödinger Operator with Singular Complex Potentials, Tech. rep., DTIC Document, 1978.
[3] G. Chen, B.G. Englert, J. Zhou, Convergence analysis of an optimal scaling algorithm for semilinear elliptic boundary value problems, Contemp. Math. 357 (2004) 69–84.
[4] G. Chen, J. Zhou, W.-M. Ni, Algorithms and visualization for solutions of nonlinear elliptic equations, Internat. J. Bifur. Chaos 10 (7) (2000) 1565–1612.
[5] G. Chen, Q. Xiong, P.J. Morris, E.G. Paterson, A. Sergeev, Y. Wang, OpenFOAM for computational fluid dynamics, Notices Amer. Math. Soc. 61 (4) (2014) 354–363.
[6] Y. Choi, P. McKenna, Numerical mountain pass methods for nonlinear boundary value problems, in: T.S. Angell, et al. (Eds.), Nonlinear Problems in Applied Mathematics, SIAM, Philadelphia, 1996, pp. 86–95.
[7] E. Dancer, The effect of domain shape on the number of positive solutions of certain nonlinear equations, J. Differential Equations 74 (1) (1988) 120–156.
[8] B. Gidas, Nirenberg, Symmetry of positive solutions of nonlinear elliptic equations in Rn, Adv. Math. Suppl. Stud. 7 (1981) 369–402.
[9] B. Gidas, W.-M. Ni, L. Nirenberg, Symmetry and related properties via the maximum principle, Comm. Math. Phys. 68 (3) (1979) 209–243.
[10] M. Grossi, et al., A uniqueness result for a semilinear elliptic equation in symmetric domains, Adv. Differential Equations 5 (1–3) (2000) 193–212.
[11] T. Ma, Remarks on an elliptic equation of Kirchhoff type, Nonlinear Anal. 63 (5) (2005) e1967–e1977.
[12] K. McLeod, Uniqueness of positive radial solutions of $\Delta u + f(u) = 0$ in Rn. II, Trans. Amer. Math. Soc. 339 (2) (1993) 495–505.
[13] J.-J. Sun, C.-L. Tang, Existence and multiplicity of solutions for Kirchhoff type equations, Nonlinear Anal. 74 (4) (2011) 1212–1222.
[14] M. Willem, Minimax Theorems, vol. 24, Springer Science & Business Media, 1997.